Applied Physics B (2022) 128:86
https://doi.org/10.1007/s00340-022-07807-w

Applied Physics B
Lasers and Optics

REGULAR PAPER

The role of wetting layer and QD-layers on the performance of 1.3 µm QD-VCSEL

Sara Alaei[1] · Mahmood Seifouri[2] · Saeed Olyaee[1] · Gholamreza Babaabbasi[3]

Received: 1 December 2021 / Accepted: 14 March 2022 / Published online: 28 March 2022
© The Author(s), under exclusive licence to Springer-Verlag GmbH Germany, part of Springer Nature 2022

Abstract

The purpose of this paper is to investigate the effect of the thickness of the wetting layer (WL) and the number of quantum dots (QDs) on the performance of 1.3 µm QD vertical-cavity surface-emitting lasers (QD-VCSELs) using self-consistent model based on rate equations and thermal conduction equations. QD-VCSELs' output power and modulation bandwidth rolled-over due to self-heating. Results demonstrate that at the same bias current, the maximum achievable 3-dB modulation bandwidth and output power are not achieved, and the point of maximum 3-dB modulation bandwidth occurred at lower currents. In addition, the larger wetting layer thickness and the greater number of QD layers modify the self-heating and enhance the efficiency and output characteristics of the laser where the rolled-over of the laser happens at higher bias currents. Furthermore, since wetting-layer thickness and the number of QD layers increase, the self-heating phenomenon is modified and the efficiency and output characteristics of the QD-VCSELs are improved by the output power rollover at higher bias currents.

1 Introduction

Vertical-cavity surface-emitting lasers (VCSELs) are receiving a lot of attention due to the applications they may have in many fields, such as optical communications, optical signal processing, and high-speed data transmission [1, 2]. It was predicted that semiconductor quantum dot (QD) lasers would offer substantial advantages over lasers of a higher dimensionality, such as quantum wells, wires, and bulks. In the case of GaAs-based VCSELs with InAs-QD structures exist many benefits such as large differential gains, thermal stability, modulation bandwidths, spectrum linewidths, and higher optical gains that result from the delta function like the discrete density of states [3, 4]. Therefore, these properties make QD-VCSELs a promising candidate for 1.3 µm advanced photonic networks [5]. The atom-like state density in QDs active region with 3-D confinement of carrier leads to increase in optical gain, reduction of threshold current, limited thermal carrier distribution, narrow spectral linewidth, and large modulation bandwidth [6–9]. Therefore, QD-VCSELs are expected to show high power, but reports indicate that the output power of these devices is limited [1, 10–13]. Consequently, QD-VCSEL performance does not fully meet expectations, since carrier confinement is severely affected by self-heating [14], which further deteriorates QD efficiency and output power [15].

The self-heating effect in QD VCSELs occurs principally due to the small diameter of the oxide aperture and the weak confinement of holes in the QD layer [16, 17]. It was determined that poor hole confinement is one of the factors limiting the output power of QD-VCSELs [18]. According to the evidence, the weak confinement of holes in InAs/GaAs QDs is likely due to thin wetting layer (WL) and close energy spacings between the holes. However, small aperture devices have a high differential resistance and a high current density, causing severe self-heating [15]. A variety of methods have been reported [6] for improving the performance of QD VCSELs [4]. These include modifying the size and location of the oxide aperture, the number of QD layers (N_L) [19], the doping concentration, and the size of the active area [15]. To improve the self-heating effect, one method is to increase the oxide aperture size [20]. Although, larger oxide apertures

✉ Saeed Olyaee
s_olyaee@sru.ac.ir

[1] Nano-Photonics and Optoelectronics Research Laboratory (NOR Lab), Shahid Rajaee Teacher Training University, Tehran, Iran

[2] Faculty of Electrical Engineering, Shahid Rajaee Teacher Training University, Tehran, Iran

[3] Faculty of Electrical Engineering, Islamic Azad University, Khorramabad, Iran

result in multimode-operation and a decrease in 3 dB modulation bandwidth of the VCSEL [21].

Another reason is due to the thin WL [15] and closely spaced hole energy levels in QDs, which can generate a self-heating effect that limits the output power [1, 15]. WL shape and thickness play a crucial role in the QD-VCSEL's performance [22–25]. So, when the active layer reaches a critical thickness and the pressure-induced growing layer begins to form 3-D islands (QDs) from 2-D monolayers, the strain is partially relaxed and the elastic energy is diminished [26]. Wetting layers (WL) are the initial monolayers that form. Thus, the 2-D WL is innately found in Stranski–Krastanow grown QD structures [27–30]. Therefore, the thin wetting layer can limit the power output in QD-VCSEL due to poor cavity confinement [15, 18]. Stranski–Krastanov (S-K) is a method for constructing In(Ga)As self-assembled QDs that has received considerable attention [31, 32]. In this method, there is an approximate 7% mismatch between InGaAs and GaAs [31, 33]. In actuality, the thickness of the WL (L_w) depends both on materials and fabrication methods [34, 35]. As a result, self-assembled QDs have a similar size, high density, and high emission efficiency [36]. In other words, self-heating severely affects the output power performance of QD VCSELs, and therefore, further investigation is needed to better understand this issue. All QD-VCSEL structural parameters have been evaluated.

To analyze the effect of self-heating on the power output of QD VCSELs, in this paper, we examine the effects of both parameters, namely the L_w and (N_L), on the performance of the 1.3 µm wavelength. In this work, the main idea is to alter the thickness of WL and number of QD layers to reduce the effect of self-heating on the QD-VCSEL, in turn improving its performance both static and dynamic. To investigate the effect of self-heating, we apply a self-consistent model based on rate equations (REs) and thermal conduction equations. By varying the number of QD layers and modifying the L_w, we can calculate the temperature increase of the active region due to the effect of self-heating as well as output power and modulation bandwidth.

2 Theoretical model

Figure 1 shows schematic cross-section diagram of QD-VCSEL emitting at 1.3 µm. Self-assembled In(Ga)As QDs are grown on GaAs substrate using a GaAs buffer layer, as illustrated in Fig. 1. The QDs are placed between the top and bottom distributed Bragg reflectors (DBRs). The DBRs consist of 33 pairs of n-doped and 22 pairs of p-doped for the bottom and the top layer, respectively. DBRs can be formed by growing $Al_{0.9}Ga_{0.1}As$ on GaAs substrate. Stranski–Krastanov growth method consists of self-assembled InGaAs QDs grown on GaAs and covered with an $In_{0.15}Ga_{0.85}As$ layer of 6 nm thickness [15, 34, 37]. A GaAs layer is used to separate the QD layers. Moreover, QDs are assumed to consist of three distinct states, where the energy gap between InGaAs and GaAs is calculated using the formula in [38].

In the next section, the injection processes are discussed in greater detail. At first, when current is injected into the active area of the QD-VCSEL, the carriers are transported from the cladding layer to the WL. Afterward, the carriers are captured by the QDs and relaxed by intra-band relaxation to the ground state. On the basis of these processes, the Appendix A contains the rate equations.

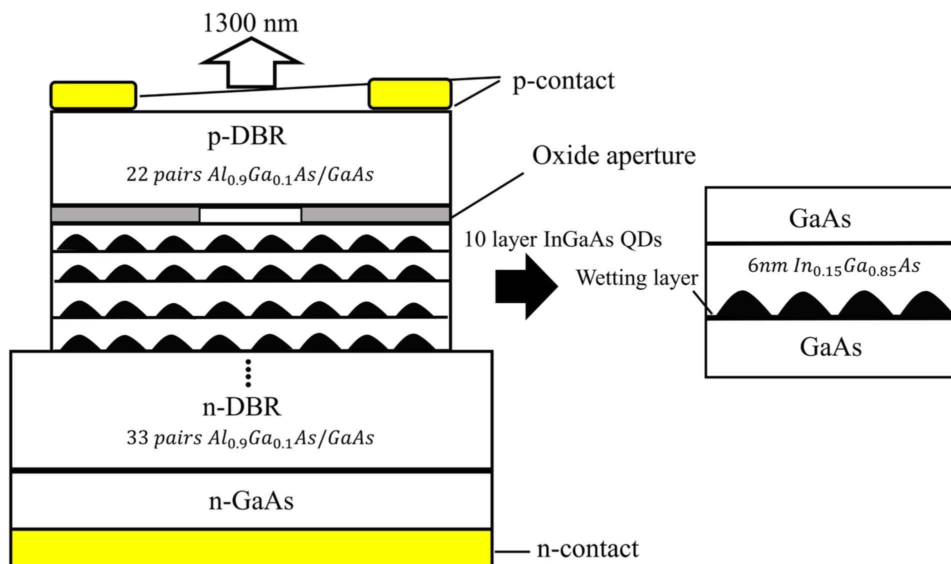

Fig. 1 Schematic cross-sectional diagram of 1.3 µm QD-VCSEL

2.1 Thermionic emission in the wetting layer

The following equation represents the carrier transport time from the cladding layer to the WL [39]:

$$t_r = \frac{L_s^2}{2D_{n.p}} \tag{1}$$

where L_s indicates the distance between the doped cladding layer and WL. D_n and D_p are the diffusion coefficient of electrons and holes, respectively, which can be calculated from the Einstein relation in [21]. t_{bw} indicates the total transport time from the cladding layer to the WL and is equal to $t_r + t_c$, and t_c represents the carrier capture time of the WL. In our calculation, t_c is chosen as 0.3 ps [21]. In general, the carrier thermionic emission time in the WL is expressed as follows [40]:

$$L_w\left(\frac{2\pi m^*}{k_B T}\right)^{1/2}\exp\left(\frac{E_{bw}}{k_B T}\right), \tag{2}$$

where, E_{bw}, m^*, and L_w are the effective energy barrier, effective mass of electrons, and the thickness of QW, respectively.T and k_B. represent temperature and Boltzmann's constant, respectively.

2.2 Carriers relaxation and escape in QDs

The capture, relaxation, and escape of carriers in QDs is governed by phonon-assisted carrier relaxation and Auger-assisted relaxation. Carrier capture is dominated by phonon-assisted relaxation, and fast intra-band relaxation of QDs is dominated by Auger-assisted relaxation [41, 42]. In addition, the complete model describes that all possible relaxation pathways. In contrast, the similar reverse pathways in the valence band corresponding to the hole relaxation [43]. Since the concentration of carriers within the wetting layer state strongly influences Auger recombination, the following formula is used to calculate the rate of carrier relaxation [41, 42]:

$$R_{ij} = A_{ij} + C_{ij}N_w \tag{3}$$

where the subscripts $i.j = 0.1.2.w$ represent the ground state, first excited state, second excited state, and the lowest state in the WL, respectively. $C_{ij}.A_{ij}$, and N_w illustrate the Auger-assisted relaxation coefficient between i_{th} and j_{th} level, the phonon-assisted relaxation rate, and carrier density in the WL(CL). The values of A_{ij}, C_{ij}, and N_w can be calculated in [21]. Consequently, the rates of carrier escape can be obtained in the condition, which the system has reached a quasi-Fermi equilibrium. Under the condition of equilibrium, the rate of escape carrier have an exponential relationship with the relaxation rates [44]. Therefore, the intra-band escape rate is calculated as follows [21]:

$$E_{sij}(i<j) = \frac{p_i}{p_j}\exp\left(-\frac{E_{ij}}{K_B T}\right)R_{ij} \tag{4}$$

The rate of escape carrier from i^{th} QD levels to WL (CL) is determined as:

$$E_{siw} = \frac{g_w}{2p_i p}\exp\left(-\frac{E_{iw}}{K_B T}\right)R_{wj}, \tag{5}$$

where, p_i and ρ are the degeneracy of the energy in the QD levels and the surface density of QDs, respectively. $E_{i.j}$ is the energy separation between different QD energy levels, and E_{iw} is the energy difference between WL state and QD levels difference between WL state and QD levels. The values of $E_{i.j}$ and E_{iw} have been extracted from [45].R_{wi} is the relaxation rate from the WL(CL) to the QD levels.

The rate equations are established in Appendix A. The parameters of the rate equations are presented in Table 1 in Appendix A. Due to the length of the cavity and the single longitudinal mode, only the central mode will be examined, and the other longitudinal modes will not be considered [15, 40]. Hence, in QD-VCSEL at 1.3 µm, the photon number S can be expressed as [15]:

$$\frac{\mathrm{d}s}{\mathrm{d}t} = \frac{\upsilon_g g_{\max}\left(f_{0e}+f_{0h}-1\right)S}{1+\varepsilon S} - \frac{S}{t_p} \tag{6}$$

where υ_g and t_p denote the group velocity, the lifetime of output photon, respectively. The cavity photon lifetime is $\left(v_g \times g_{th}\right)^{-1}$, where g_{th} (threshold gain) can be obtained through $g_{th} = a_i + a_m$. a_i is the intrinsic losses and the mirror losses is $a_m = \left(\frac{1}{2L_{cav}}\right)Ln\left(\frac{1}{R_t R_b}\right)$ in which L_{cav} is the cavity length and R_t and R_b are the of the top and bottom reflectivity Bragg mirrors, respectively. $\left(f_{0e}+f_{0h}-1\right)$ indicates the degree of population inversion. $\varepsilon = \frac{\varepsilon_m}{\Gamma v_a}$, where Γ and v_a are the optical confinement factor and the volume of all QDs. ε_m is the coefficient of nonlinear gain which can be extracted from [46]. $g_{\max}$ in Eq. (6) is the maximum model gain, which can be expressed as [3, 47]:

$$g_{\max} = \frac{\hbar q}{c n_r m_0 \varepsilon_0}\frac{\left|P_{cv}\right|^2}{m_0 E_L}\frac{\rho \Gamma_r}{d_D}\sqrt{2\pi}\left(\frac{2.35}{F_{in}}\right) \tag{7}$$

where $\left|P_{cv}\right|^2$ is the transition matrix, which can be expressed in [3] and d_D and F_{in} represent the effective thickness of QD layer and the full-width at half-maximum (FWHM) of the inhomogenous broadening of QDs, respectively, where FWHM is dependent on τ_p [16, 48]. Accordingly, the QD-VCSEL operates in a single mode (coherently) with an

Table 1 Parameter used in the equations

Symbol	Meaning	Value
$f_i\,(i = B.w.0.1.2)$	Carrier occupation probability in the barrier, WL (CL), QD ground state, first excited state and second excited state, respectively	
N_B	Carrier concentration in the barrier layer	
J	Injected current density	
q	Electronic charge	1.60×10^{-19}C
b	Total thickness of GaAs	191 nm
n	Number of QD layers	
K_B	Boltzmann's constant	1.38×10^{-5}J/K
T	Temperature at the center of active region	
$p_i(i = 0.1.2)$	Degeneracy of QD levels	$p_0 = 1.p_1 = 2.p_2 = 4$
S_a	Area of active region	78.53 μm^2
E_L	Lasing energy	0.957 eV
S	Photon number in cavity	
F_{in}	FWHM of QD inhomogeneous broadening	24 meV
F_{ho}	FWHM of QD homogeneous broadening	15 meV
g_w	Parameter describing the carrier concentration in the WL (CL)	[21]
t_{bw}	Carrier transport time from cladding layer to the nearest WL (CL), which is a function of temperature	[21]
t_c	Carrier capture time	0.3 ps
t_{ewb}	Carrier escape time from WL (CL) to the GaAs barrier, which is a function of temperature	[21]
$g_{\max}$	Maximum modal gain of QD laser	
n_r	Refractive index of active material	3.409
m_0	Rest mass of electron	9.1×10^{-31}Kg
h	Planck's constant	6.62×10^{-34}Js
v_D	Volume of one QD	$1.6 \times 10^{-24} m^3$
t_p	Photon lifetime	

FWHM of 24 meV and a sidemode suppression ratio of 28 dB [13].

2.3 Thermal conduction equation

In semiconductor lasers, many parameters are affected by temperature, so the thermal analysis is very complicated. One of the dominant heat sources in QD-VCSELs is the active region, where heat is generated by non-radiative recombination and spontaneous emission [49]. Therefore, the steady-state thermal density at the active region is expressed as [50, 51]:

$$Q_a(j) = \frac{V(T)\left(1 - \eta_{sp} f_{sp}\right)}{n d_D}\left\{J_{th}(T) + \left[J - J_{th}(T)\right]\left(1 - \eta_{QD}\right)\right\} \tag{8}$$

where, η_{sp} and f_{sp} are the spontaneous quantum efficiency and spontaneous radiation escape factor [50]. η_{QD} is the internal quantum efficiency of the device that can be obtained from [15].$V(T)$ is the voltage at the center of the active area, which can be calculated from the following equation [51]:

$$V(T) = \frac{2k_B T}{q}\left(ln\frac{J}{J_s} + \frac{r_0}{r_{01}}\right) \tag{9}$$

where, J_s is the reversed saturation current density. r_0 and r_{01} are the radius of the oxide aperture and the device radius, respectively.

We assume that no heat escapes through the sides, the edge, or the top of the device. The temperature change with time (t) in the device can be governed by three-dimensional dynamic thermal equation [52]:

$$(r.t) = \frac{1}{r}\frac{\partial}{\partial r}\left[r\frac{\partial T(r.t)}{\partial r}\right] + \frac{1}{\lambda_i}Q(J.r.t), \tag{10}$$

where, k_i, λ_i., and r represent the thermal diffusion coefficient, effective thermal conductivity, and radius, respectively. Equation (10) can be solved using Green's function [15, 52].

Table 2 Physical properties of the structure

Symbol	Meaning	Value
S_P	Area of p-contact region	3.77×10^{-5}cm^2
S_n	Area of n-contact region	2.5×10^{-3}cm^2
ρ_P	Resistivity of p-doped DBR	0.23 Ωcm
ρ_n	Resistivity of n-doped DBR	0.032 Ωcm
r_0	Radius of oxide aperture	6 μm
r_{01}	Radius of device	40 μm
f_{sp}	Spontaneous radiation escape factor	10 nm
η_{sp}	Spontaneous quantum efficiency	0.667
η_{QD}	Internal quantum efficiency of PhC-VCSEL	0.5
k_i	Thermal diffusion coefficient	
	GaAs	0.267 cm^{-2}s^{-1}
	$Al_{0.9}Ga_{0.1}As$	0.521 cm^{2}s^{-1}
λ_i	Thermal conduction coefficient	
	GaAs	44 WmK
	$Al_{0.9}Ga_{0.1}As$	25.5 WmK
J_s	Reverse saturation current density	6×10^{-5}Am^{-2}

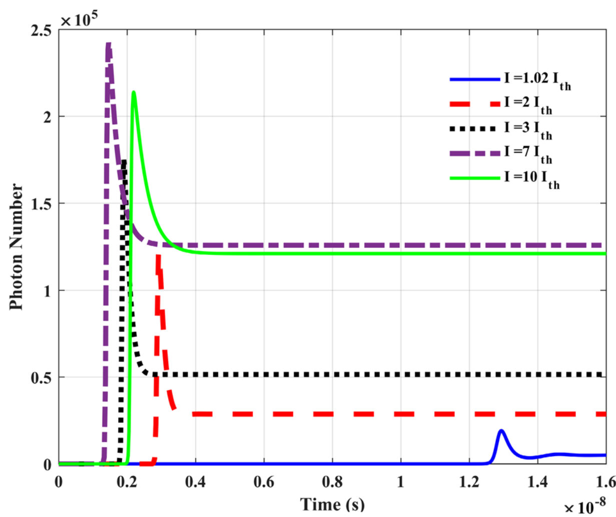

Fig. 2 The output photon number at different injection current values

Joule heating in the DBR stacks is another source of heat in QD-VCSELs, which leads to severe self-heating. The Joule heat density can be calculated according to [51]. The values of the used parameters are listed in Table 2 in Appendix A.

3 Results and discussion

In this section, the effects of parameters such as L_w and N_L on output power, the probability of carrier occupation, and the 3-dB modulation bandwidth are examined in more detail.

The number of output photons at different currents can be determined by simultaneously solving the rate equation and the thermal conduction equation for QD-VCSELs. As illustrated in Fig. 2, the number of output photons varies with different currents. The value of threshold current 0.7 mA was acquired at the N_L of 10, and the surface density of 5×10^{14}m^{-2} at 300 K. Because the number of carriers is small at currents near the threshold, the turn-on delay is high. As should be emphasized, the reducing turn-on delay of QD-VCSELs is not permanent with increasing current. Threshold current increases with increasing injection current and temperature since the threshold current is strongly influenced by temperature. Therefore, increasing the threshold current leads to a delay in reaching the steady state and consequently causes a turn-on delay. According to Fig. 2, when the current becomes higher, the temperature rises and QD-VCSELs operate slower, which is because of the effect of self-heating and output power roll-over.

According to previous studies [15], it has been found that the confinement of holes depends on the thickness of the wetting layer, and therefore the thermionic emission time depends on the wetting layer thickness. Increasing the L_w leads to an increase in the number of holes in this layer as well as an increase in thermionic emission time.

Figure 3 shows the characteristics of output power and the probability of electron and hole occupation at the ground state of QD-VCSELs as a function of current for varying L_w. According to our studies of the effect of L_w on the static behavior of the QD-VCSEL, increasing the wetting layer thickness delays the roll-over of output power at higher currents and output powers. Moreover, Fig. 3 illustrates how increasing the wetting layer thickness enhances the probability of holes occupation, and this causes power roll-over to occur over a broad range of currents, which results in improved output power.

Figure 4 shows the power efficiency as the function of the injection current for the different values of L_W with N_L=10 at room temperature. The behavior of power efficiency for a different value of L_w is very similar to that of power roll-over, while in the maximum value of L_w, power efficiency increases. Consequently, the VCSEL with = L_w 1 nm has the highest power efficiency.

The effect of injection current on the temperature increase at the center of the active region is shown in Fig. 5. It can also be observed that, an increase in the L_w leads to increase thermionic emission in the wetting layer as well as greater confinement of holes. As a consequence, the temperature due to self-heating increases at a slower rate, which improves the effect of self-heating in the active area.

To examine the effect of the number of QD layers on the operation of the 1.3 μm QD-VCSEL, N_L is chosen to be 10, 15, 18, and 20 respectively. As shown in Fig. 6, the electron and hole occupation probabilities in the ground

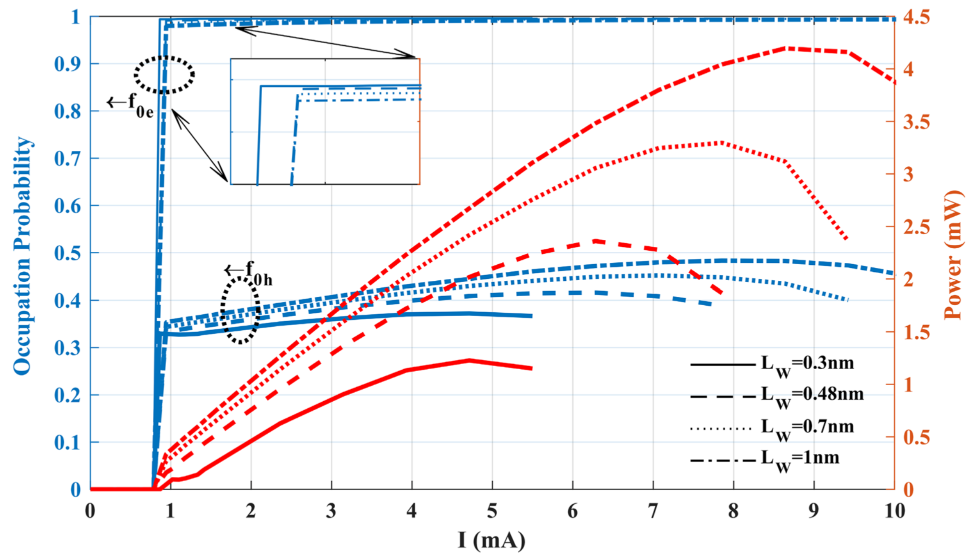

Fig. 3 Effect of the L_w on the output power and occupation probability

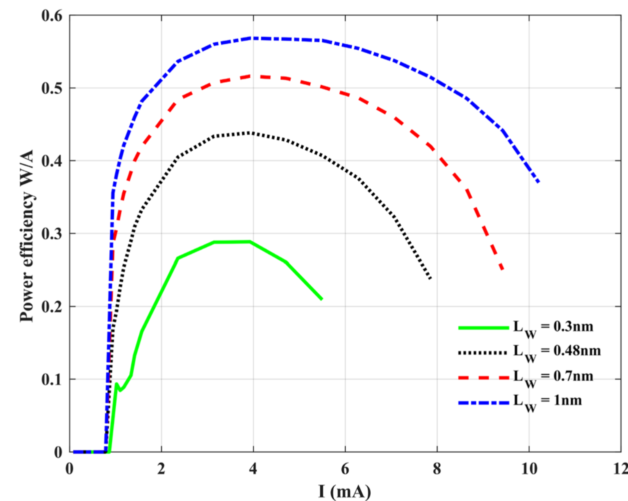

Fig. 4 The Power efficiency versus the current for a different values of L_w with N_L=10 at the room temperature

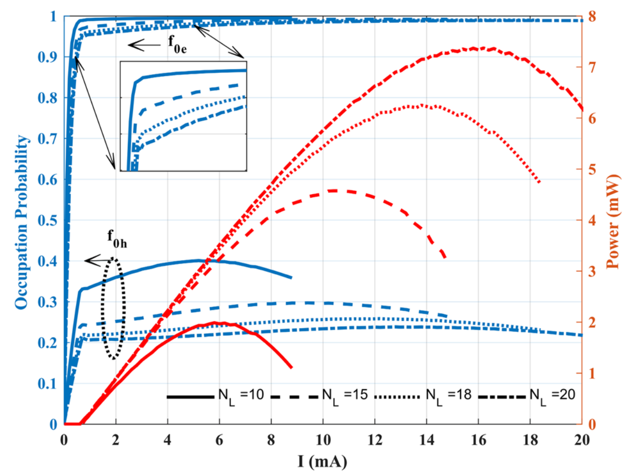

Fig. 6 Effect of the N_L on the output power and occupation probability

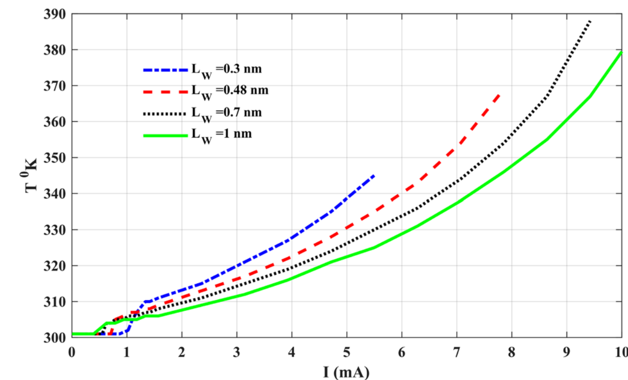

Fig. 5 Effect of the L_w on the temperature increase of the 1.3 μm VCSEL active region for different injection currents

state, as well as output power are plotted as a function of the injected current for 1.3 μm QD-VCSEL (F_0-I-P_{out}). Here, we investigate the effect of N_L on self-heating. Therefore, output power (P_{out}) could be calculated at different current, as shown in Fig. 6. According to the simulation, increasing the N_L in results to delaying the output power roll-over in the higher injection current, which is due to the improved self-heating effect. Due to the self-heating effect, there is also the roll-over of occupation probability in addition to the output power roll-over. Also, this figure illustrates the importance of the self-heating effect on carrier occupation probabilities in QD ground states. According to this figure, as the N_L increases, the occupation probability of holes decreases. Therefore, self-heating results in an increase in temperature in the active region, which leads to more carriers escaping,

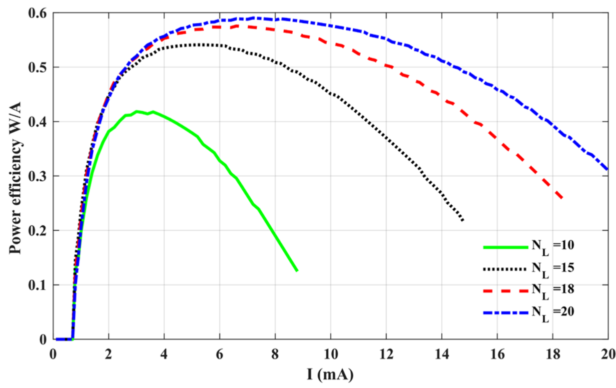

Fig. 7 The Power efficiency versus the current for a different values of N_L with L_w=0.48 nm at the room temperature

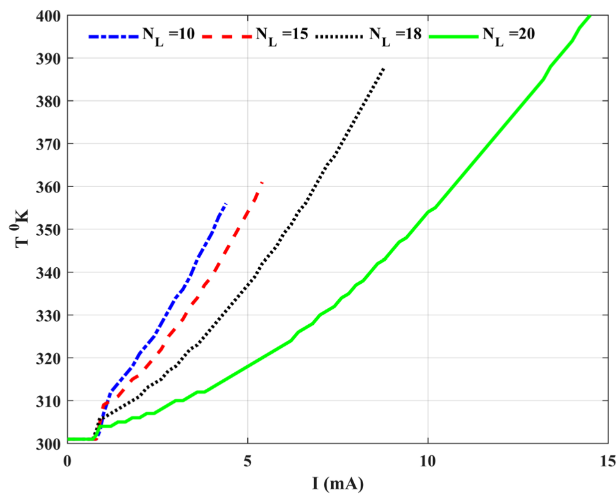

Fig. 8 Effect of the N_L on the temperature increase of the 1.3 µm VCSEL active region for different injection currents

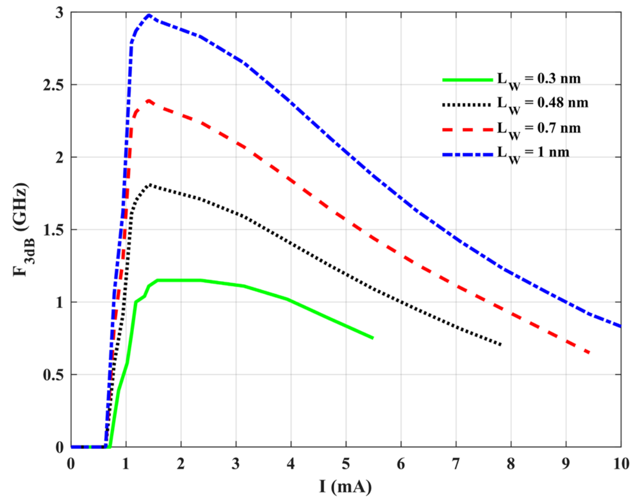

Fig. 9 Effect of L_w on the 3-dB modulation bandwidth of VCSELs at 1.3 µm as a function of the bias current

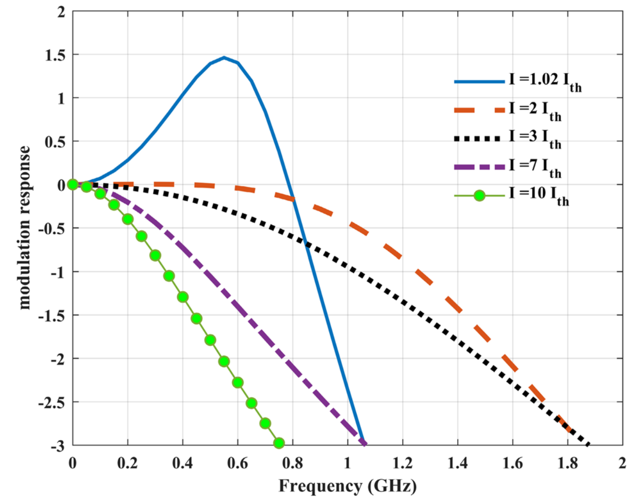

Fig. 10 The modulation response at different injection current

especially holes. From Fig. 6, it is evident that the effect of self-heating is greater on the occupation probability of holes than electrons.

In Fig. 7 power efficiency is shown as a function of injection current for different values of N_L with L_w=0.48 nm at room temperature. In varying values of N_L, power efficiency behaves very similar to power rollover, and power efficiency increases at the maximum value of N_L. Consequently, the VCSEL with N_L=20 has the highest power efficiency.

Figure 8 shows the calculation of the temperature of the active region as a function of the injection current for different numbers of QD layers. It is evident that increasing the N_L can significantly improve the effect of self-heating. The results show that when the N_L reach 20 layers, the self-heating effect occurs at a slower rate.

The modulation response of QD-VCSELs as a function of current considering the effect of self-heating at different L_w is depicted in Fig. 9. It is evident from Fig. 9 that increasing the L_w increases the maximum modulation bandwidth. As an example, when the current is between 1 and 2 mA and L_w = 1nm, the best frequency response occurs, which results in more power in the highest modulation response.

The modulation response of a QD-VCSEL is shown in Fig. 10 at various bias currents. It can be concluded that the maximum 3-dB bandwidth is obtained at bias currents about $3I_{th}$. Any further increase in bias current will lead to a deterioration of the 3-dB bandwidth of the QD-VCSEL.

Figure 11 shows the 3-dB modulation bandwidth of the QD-VCSEL as a function of the injection current with different QD layers. It is obvious that the maximum bandwidth

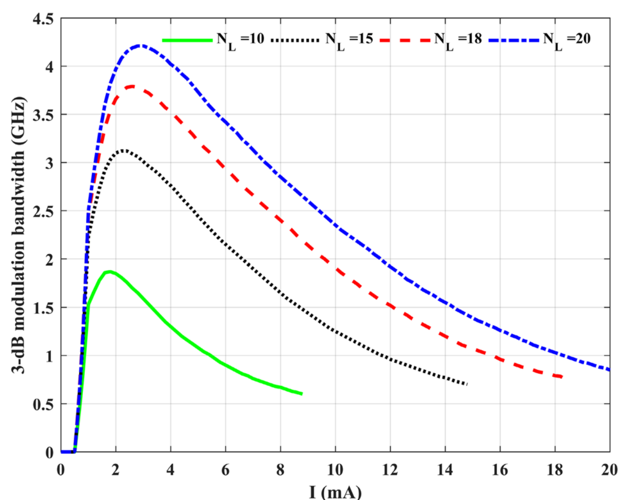

Fig. 11 Effect of the N_L on the 3-dB modulation bandwidth of VCSELs at 1.3 µm as a function of the bias current

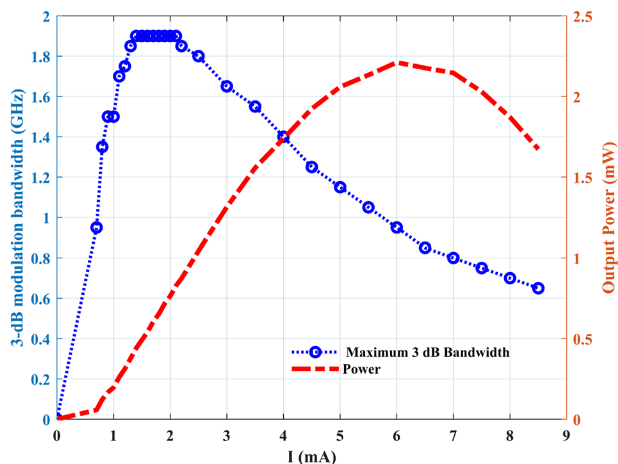

Fig. 12 The 3-dB modulation bandwidth and output power of the QD-VCSEL as a function of bias current

increases when the N_L increases. Consequently, the best modulation bandwidth occurs when $N_L\hat{>}20$ and the injection current is between 2 and 4 mA.

To investigate the performance of the 1.3 µm QD-VCSEL, we have calculated the maximum modulation bandwidth and output power as a function of the bias current for $N_L = 10$ and L_w=0.48 nm. According to Fig. 12, as the injection current increases, the 3-dB modulation bandwidth also increases and reaches its maximum value at ~ $3I_{th}$. A further increase in bias current results in the reduction of 3-dB modulation bandwidth. However, the maximum output power can be achieved at higher bias currents (about $6I_{th}$). Therefore, maximum power and modulation bandwidth cannot both be achieved simultaneously. This behavior can be attributed to the effect of QD-VCSELs self-heating, which drastically increases the escape rate of carriers especially the holes. Consequently, it can be seen that the threshold current increases sharply, which has a negative impact on the dynamic and static properties of QD-VCSELs. For example, at the highest output power, the 3-dB modulation response is as low as 1 GHz, and the maximum bandwidth corresponds to 0.6 mW output power, which limits the performance of the laser.

4 Conclusion

Due to self-heating and temperature increase, QD-VCSELs' output power and modulation bandwidth decrease. At the same bias current, the maximum achievable 3-dB modulation bandwidth and output power are not achieved, and the point of maximum 3-dB modulation bandwidth occurred at lower currents. As a result, the laser performance can be improved by a self-heating rein. Increasing the thickness of the wetting layer and the number of QD layers in the active region contribute to the enhancement of the self-heating of the laser, which allows the rollover to occur at higher bias currents. As the wetting layer thickness increases, the maximum output power increases from about 1.4 mW to 4.2 mW, while the maximum modulation bandwidth increases from about 1.2 GHz to 3 GHz. Furthermore, it resulted in improved laser characteristics due to a greater number of QD layers. An output power up to 7 mW and modulation bandwidth up to 3 GHz in 20 QD-layer structures can be achieved.

Appendix A: rate equations

Here, the rate equations for the 1.3 µm QD-VCSELs are listed [15, 21]. The parameters of the rate equations are demonstrated in Table 1.

$$\frac{dN_B}{dt} = \frac{J}{qb} + \frac{1}{t_{ewb}}\frac{g_w f_w}{\frac{b}{n}}\left(1 - f_B\right) - \left(\frac{1}{t_{bw}} + \frac{1}{t_{rB}}\right)N_B \quad \text{(A1)}$$

$$\frac{df_w}{dt} = \frac{(1-f_w)}{g_w}\frac{N_B b/n}{t_{bw}} - \frac{f_w}{t_{ebw}} + \sum_{i=0}^{n2}\left[\frac{2P_i\rho}{g_w}Es_{iw}f_i(1-f_w) - R_{wi}f_w(1-f_i)\right] - \frac{f_w}{t_{rw}} \quad \text{(A2)}$$

$$\frac{df_2}{dt} = \frac{g_w}{2p_2\rho}R_{w2}f_w(1-f_2) - Rs_{2w}f_2(1-f_w) + \sum_{i=0}^{1}\left[\frac{p_i}{p_2}Es_{i2}f_i(1-f_2) - R_{2i}f_2(1-f_i)\right] - \frac{f_2}{t_{r2}} \quad \text{(A3)}$$

$$\frac{df_1}{dt} = \frac{g_w}{2p_1\rho}R_{w1}f_w(1-f_1) - Es_{1w}f_1(1-f_w) + \left[\frac{p_2}{p_1}R_{21}f_2(1-f_1) - Es_{12}f_1(1-f_2)\right] + \left[\frac{p_0}{p_1}Es_{01}f_0(1-f_1) - R_{10}f_1(1-f_0)\right] - \frac{f_1}{t_{r1}} \quad \text{(A4)}$$

$$\frac{df_0}{dt} = \sum_{i=1}^{2n}\left[\frac{p_i}{p_0}R_{i0}f_i(1-f_0) - Es_{0i}f_0(1-f_i)\right] + \left[\frac{g_w}{2p_0\rho}R_{w0}f_w(1-f_0) - Es_{0w}f_0(1-f_w)\right] - \frac{f_0}{t_{r0}} - \frac{1}{2p_0 n S_a \rho}\frac{\upsilon_g g_{\max}(f_{0e}+f_{0h}-1)}{1+\varepsilon S} \quad \text{(A5)}$$

Acknowledgements This work has been done in Nano-photonics and Optoelectronics Research Laboratory (NORLab), Shahid Rajaee University.

Authors' contributions All authors read and approved the final manuscript.

Funding Not Applicable.

Availability of data and material Not applicable.

Code availability Not applicable.

Declarations

Conflicts of interest The authors declare that they have no known competing financial interests or personal relationships that could have appeared to influence the work reported in this paper.

Ethics approval The authors declared that the manuscript ethics is approved as per the journal.

Consent to participate Yes.

Consent for publication The authors gave consent for publication as per the journal standard.

References

1. C. Tong, X. Dawei, S.F. Yoon, Y. Ding, W.J. Fan, Temperature characteristics of 1.3-μm p-doped InAs–GaAs quantum-dot vertical-cavity surface-emitting lasers. IEEE J. Sel. Top. Quantum Electron. **15**(3), 743–748 (2009)
2. C.W. Wilmsen, H. Temkin, L.A. Coldren, *Vertical-cavity surface-emitting lasers: design, fabrication, characterization, and applications*, vol. 24 (Cambridge University Press, 2001)
3. K. Mukai, Y. Nakata, K. Otsubo, M. Sugawara, N. Yokoyama, H. Ishikawa, 1.3-μm CW lasing characteristics of self-assembled InGaAs-GaAs quantum dots. IEEE J. Quantum Electron. **36**(4), 472–478 (2000)
4. R.P. Sarzala, Modeling of the threshold operation of 1.3-μm GaAs-based oxide-confined (InGa) As-GaAs quantum-dot vertical-cavity surface-emitting lasers. IEEE J. Quantum Electron. **40**(6), 629–639 (2004)
5. N. Ledentsov, Long-wavelength quantum-dot lasers on GaAs substrates: from media to device concepts. IEEE J. Sel. Top. Quantum Electron. **8**(5), 1015–1024 (2002)
6. Y. Arakawa, H. Sakaki, Multidimensional quantum well laser and temperature dependence of its threshold current. Appl. Phys. Lett. **40**(11), 939–941 (1982)
7. M. Asada, Y. Miyamoto, Y. Suematsu, Gain and the threshold of three-dimensional quantum-box lasers. IEEE J. Quantum Electron. **22**(9), 1915–1921 (1986)
8. H. Sakaki, Quantum wire superlattices and coupled quantum box arrays: A novel method to suppress optical phonon scattering in semiconductors. Jpn. J. Appl. Phys. **28**(2A), L314 (1989)
9. K.J. Vahala, Quantum box fabrication tolerance and size limits in semiconductors and their effect on optical gain. IEEE J. Quantum Electron. **24**(3), 523–530 (1988)
10. Y.H. Chang, P.C. Peng, W.K. Tsai, G. Lin, R.S. Hsiao, H.P. Yang, H.C. Yu, K.F. Lin, J.Y. Chi, S.C. Wang, H.C. Kuo, Single-mode monolithic quantum-dot VCSEL in 1.3 μm with sidemode suppression ratio over 30 dB. IEEE Photon. Technol. Lett. **18**(7), 847–849 (2006)
11. N.N. Ledentsov, F. Hopfer, D. Bimberg, High-speed quantum-dot vertical-cavity surface-emitting lasers. Proc. IEEE **95**(9), 1741–1756 (2007)
12. J. Lott, N.N. Ledentsov, V.M. Ustinov, N.A. Maleev, A. Zhukov, A. Kovsh, M.V. Maximov, B.V. Volovik, Zh.I. Alferov, D. Bimberg, Inas-ingaas quantum dot vcsels on gaas substrates emitting at 1.3-μm. Electron. Lett. **36**(16), 1384–1385 (2000)
13. H.-C. Yu, J.S. Wang, Y. Su, S.J. Chang, F.I. Lai, Y.H. Chang, H.C. Kuo, C.P. Sung, H.D. Yang, K.F. Lin, J.M. Wang, J. Chi, R. Hsiao, S. Mikhrin, 1.3-μm InAs-InGaAs quantum-dot vertical-cavity surface-emitting laser with fully doped DBRs grown by MBE. IEEE Photon. Technol. Lett. **18**(2), 418–420 (2006)
14. D. Boiko, G. Guerrero, E. Kapon, Thermoelectrical model for vertical cavity surface emitting lasers and arrays. J. Appl. Phys. **100**(10), 103102 (2006)
15. D. Xu, S.F. Yoon, C. Tong, Self-consistent analysis of carrier confinement and output power in 1.3-μm InAs–GaAs quantum-dot VCSELs. IEEE J. Quantum Electron. **44**(9), 879–885 (2008)
16. Y. Liu, W.C. Ng, K.D. Choquette, K. Hess, Numerical investigation of self-heating effects of oxide-confined vertical-cavity surface-emitting lasers. IEEE J. Quantum Electron. **41**(1), 15–25 (2005)
17. T. Wipiejewski, H.D. Wolf, L. Korte, W. Huber, G. Kristen, C. Hoyler, H. Hedrich, O. Kleinbub, M. Popp, J. Kaindl, and A. Rieger, Performance and Reliability of Oxide Confined

VCSELs. in 1999 Proceedings. 49th Electronic Components and Technology Conference (Cat. No. 99CH36299). 1999. IEEE.
18. D.W. Xu, C.Z. Tong, S.F. Yoon, L.J. Zhao, Y. Ding, W.J. Fan, Self-heating effect in 1.3-μm p-doped InAs/GaAs quantum dot vertical cavity surface emitting lasers. J. Appl. Phys. **107**(6), 063107 (2010)
19. S. Alaei, M. Seifouri, S. Olyaee, and G. Babaabbasi, Effect of the Number of Quantum-Dot Layers on the Performance of the 1.3 μm InAs/GaAs VCSELs. in 2021 29th Iranian Conference on Electrical Engineering (ICEE). 2021. IEEE.
20. D.W. Xu, S.F. Yoon, Y. Ding, C.Z. Tong, W.J. Fan, L.J. Zhao, 13-μm in (Ga) as quantum-dot VCSELs fabricated by dielectric-free approach with surface-relief process. IEEE Photon. Technol. Lett. **23**(2), 91–93 (2010)
21. C.Z. Tong, S.F. Yoon, C.Y. Ngo, C.Y. Liu, W.K. Loke, Rate equations for 13-μm dots-under-a-well and dots-in-a-well self-assembled InAs–GaAs quantum-dot lasers. IEEE J. Quantum Electron. **42**(11), 1175–1183 (2006)
22. D. Deppe, D. Huffaker, Quantum dimensionality, entropy, and the modulation response of quantum dot lasers. Appl. Phys. Lett. **77**(21), 3325–3327 (2000)
23. D.R. Matthews, H.D. Summers, P.M. Smowton, M. Hopkinson, Experimental investigation of the effect of wetting-layer states on the gain–current characteristic of quantum-dot lasers. Appl. Phys. Lett. **81**(26), 4904–4906 (2002)
24. S. Sanguinetti, M. Henini, M.G. Alessi, M. Capizzi, P. Frigeri, S. Franchi, Carrier thermal escape and retrapping in self-assembled quantum dots. Phys. Rev. B **60**(11), 8276 (1999)
25. L. Wang, V. Křápek, F. Ding, F. Horton, A. Schliwa, D. Bimberg, A. Rastelli, O.G. Schmidt, Self-assembled quantum dots with tunable thickness of the wetting layer: role of vertical confinement on interlevel spacing. Phys. Rev. B **80**(8), 085309 (2009)
26. D.-S. Han, L.V. Asryan, Effect of the wetting layer on the output power of a double tunneling-injection quantum-dot laser. J. Lightwave Technol. **27**(24), 5775–5782 (2009)
27. J.S. Kim, I.-H. Bae, Optical properties of wetting layer in InAs quantum dots at dierent growth temperatures. J. Korean Phys. Soc. **42**, S483–S486 (2003)
28. R. Leon, Y. Kim, C. Jagadish, M. Gal, J. Zou, D.J.H. Cockayne, Effects of interdiffusion on the luminescence of InGaAs/GaAs quantum dots. Appl. Phys. Lett. **69**(13), 1888–1890 (1996)
29. K. Nishi, R. Mirin, D. Leonard, G. Medeiros-Ribeiro, P.M. Petroff, A.C. Gossard, Structural and optical characterization of InAs/InGaAs self-assembled quantum dots grown on (311) B GaAs. J. Appl. Phys. **80**(6), 3466–3470 (1996)
30. A. Patanè, A. Polimeni, P.C. Main, M. Henini, L. Eaves, High-temperature light emission from InAs quantum dots. Appl. Phys. Lett. **75**(6), 814–816 (1999)
31. R. Kumar, Y. Maidaniuk, S.K. Saha, Y.L. Mazur, G.J. Salamo, Evolution of InAs quantum dots and wetting layer on GaAs (001): Peculiar photoluminescence near onset of quantum dot formation. J. Appl. Phys. **127**(6), 065306 (2020)
32. S. Lee, O.L. Lazarenkova, P. von Allmen, F. Oyafuso, G. Klimeck, Effect of wetting layers on the strain and electronic structure of InAs self-assembled quantum dots. Phys. Rev. B **70**(12), 125307 (2004)
33. M. Shahzadeh, M. Sabaeian, The effects of wetting layer on electronic and optical properties of intersubband P-to-S transitions in strained dome-shaped InAs/GaAs quantum dots. AIP Adv. **4**(6), 067113 (2014)
34. A. Baskaran, P. Smereka, Mechanisms of stranski-krastanov growth. J. Appl. Phys. **111**(4), 044321 (2012)
35. H. Zhang, Y. Chen, G. Zhou, C. Tang, Z. Wang, Wetting layer evolution and its temperature dependence during self-assembly of InAs/GaAs quantum dots. Nanoscale Res. Lett. **7**(1), 1–6 (2012)
36. K. Kash, A. Scherer, J.M. Worlock, H.G. Craighead, M.C. Tamargo, Optical spectroscopy of ultrasmall structures etched from quantum wells. Appl. Phys. Lett. **49**(16), 1043–1045 (1986)
37. V. Shchukin, N.N. Ledentsov, D. Bimberg, *Epitaxy of nanostructures* (Springer Science & Business Media, 2004)
38. X. Han, J. Li, J. Wu, G. Cong, X. Liu, Q. Zhu, Z. Wang, Intersubband optical absorption in quantum dots-in-a-well heterostructures. J Appl. Phys. **98**(5), 053703 (2005)
39. N. Tansu, L.J. Mawst, Current injection efficiency of InGaAsN quantum-well lasers. J Appl. Phys. **97**(5), 054502 (2005)
40. H. Abbaspour, V. Ahmadi, M.H. Yavari, Analysis of QD VCSEL dynamic characteristics considering homogeneous and inhomogeneous broadening. IEEE J. Sel. Top. Quantum Electron. **17**(5), 1327–1333 (2011)
41. Q. Cao, S.F. Yoon, C.Z. Tong, C.Y. Ngo, C.Y. Liu, R. Wang, H.X. Zhao, Two-state competition in 1.3 μ m multilayer InAs/InGaAs quantum dot lasers. Appl. Phys. Lett. **95**(19), 191101 (2009)
42. A.V. Uskov, F. Adler, H. Schweizer, M.H. Pilkuhn, Auger carrier relaxation in self-assembled quantum dots by collisions with two-dimensional carriers. J. Appl. Phys. **81**(12), 7895–7899 (1997)
43. A. Steinhoff, H. Kurtze, P. Gartner, M. Florian, D. Reuter, A.D. Wieck, M. Bayer, F. Jahnke, Combined influence of Coulomb interaction and polarons on the carrier dynamics in InGaAs quantum dots. Phys. Rev. B **88**(20), 205309 (2013)
44. R. Lang, Problems in recent analysis of injected carrier dynamics in semiconductor quantum dots. Appl. Phys. Lett. **79**(24), 3912–3913 (2001)
45. E. Xing, C. Tong, J. Rong, S. Shu, H. Wu, L. Wang, S. Tian, L. Wang, Modulation of carrier dynamics and threshold characteristics in 1.3-μm quantum dot photonic crystal nanocavity lasers. Opt. Laser Technol. **82**, 10–16 (2016)
46. R. Bose, J.S. Pelc, S. Vo, C.M. Santori, R.G. Beausoleil, Carrier dynamics in GaAs photonic crystal cavities near the material band edge. Opt. Express **23**(10), 12732–12739 (2015)
47. Y. Nakata, Y. Sugiyama, M. Sugawara, *Semiconductors and semimetals* (Academic, New York, 1999)
48. A.F.J. Levi, *Applied quantum mechanics* (Cambridge University Press, 2006)
49. T. Kobayashi, Y. Furukawa, Temperature distributions in the GaAs-AlGaAs double-heterostructure laser below and above the threshold current. Jpn. J. Appl. Phys. **14**(12), 1981 (1975)
50. W. Nakwaski, M. Osinski, Thermal properties of etched-well surface-emitting semiconductor lasers. IEEE J. Quantum Electron. **27**(6), 1391–1401 (1991)
51. H. Zhang, G. Mrozynski, A. Wallrabenstein, J. Schrage, E. Griese, Self-consistent model and numerical analysis of VCSEL's laser diodes. Int. J. Infrared Millimeter Waves **24**(3), 377–389 (2003)
52. Y.-G. Zhao, J. McInerney, Transient temperature response of vertical-cavity surface-emitting semiconductor lasers. IEEE J. Quantum Electron. **31**(9), 1668–1673 (1995)

Publisher's Note Springer Nature remains neutral with regard to jurisdictional claims in published maps and institutional affiliations.